Eur. Phys. J. C (2025) 85:1094
https://doi.org/10.1140/epjc/s10052-025-14801-x

THE EUROPEAN PHYSICAL JOURNAL C

Regular Article - Theoretical Physics

Triple gauge coupling analysis using boosted W's and Z's

O. J. P. Éboli[1,a], **Tathagata Ghosh**[2,b], **Matheus Martines**[1,c], **Sujay Shil**[1,d]

[1] Instituto de Física, Universidade de São Paulo, São Paulo, São Paulo 05580-090, Brazil
[2] Regional Centre for Accelerator-Based Particle Physics, Harish-Chandra Research Institute, A CI of Homi Bhabha National Institute, Chhatnag Road, Jhunsi, Allahabad 211019, India

Received: 16 July 2025 / Accepted: 16 September 2025

Abstract We analyze the Large Hadron Collider potential to study triple couplings of the electroweak gauge bosons using their boosted hadronic decays. Deviations from Standard Model predictions spoil cancelations present in the Standard Model leading to the growth of the electroweak diboson production cross section at high center-of-mass energies. In this kinematical limit, W's and Z's are highly boosted, and consequently, their hadronic decays give rise to fat jets. Here, we show that the study of boosted hadronically decaying W and Z leads to limits on triple gauge couplings that are comparable to the ones originating from the leptonic decay channels.

1 Introduction

The CERN Large Hadron Collider (LHC) has already accumulated a substantial dataset allowing for precision tests of the Standard Model (SM) and searches for new physics. Within the SM framework, the triple and quartic vector-boson couplings are determined by the non-abelian $SU(2)_L \otimes U(1)_Y$ gauge symmetry, being completely fixed in terms of the gauge couplings. Possible deviations from the SM predictions for the triple gauge couplings (TGC) are a clear sign of new physics and consequently, TGCs are investigated at the LHC in charged processes like W^+W^-, $W^\pm Z$ and $W^\pm\gamma$ productions.

Due to the importance of TGC measurements, the ATLAS and CMS collaborations conduct studies on the electroweak TGC through various processes. They analyze the $W^\pm Z \to \ell^+\ell^-\ell'^\pm + E_T^{\rm miss}$ channel [1,2] as well as the $W^+W^- \to \ell^+\ell^{(\prime)-} + E_T^{\rm miss}$ final state [3,4]. Additionally, TGC were investigated in the $W^\pm\gamma \to \ell^\pm\gamma + E_T^{\rm miss}$ production [5]. The ATLAS collaboration further explored the semileptonic reaction $WW/WZ \to \ell\nu qq'$ at 8 TeV [6] to extract limits on anomalous TGCs, with the most stringent constraints arising from cases where a single fat jet was tagged as a W or Z boson.

In this work, we analyze the WW/WZ and $W\gamma$ diboson productions in the fully hadronic final state, focusing on scenarios where the boosted W/Z bosons are identified as high transverse momentum and large-radius jets. We utilize the large-radius jet mass and its substructure to effectively characterize the hadronically decaying W/Z bosons and to reduce Standard Model backgrounds. To demonstrate the potential of these new channels for TGC studies, we recast the ATLAS searches for heavy resonances decaying into WW/WZ in the hadronic channel [7] as well as $W\gamma$ [8]. We show that these processes can lead to TGC bounds comparable to the ones obtained by studying leptonic final states. Moreover, we also analyze the potential of the High Luminosity LHC (HL-LHC) run to probe anomalous TGC in all-hadronic electroweak diboson (EWDB) channels, *i.e.* in the production of pairs WZ, WW and $W\gamma$.

This work is organized as follows: in Sect. 2 we present the adopted theoretical framework as well as the analyses methodology. Section 3 contains our results and we summarize our conclusions in Sect. 4.

2 Analysis framework

Assuming the existence of a mass gap between the new physics energy scale and the electroweak one, we parametrize the deviations from the SM TGC predictions using effective field theory. Furthermore, conjecturing that the scalar particle observed in 2012 [9,10] belongs to an electroweak doublet,

[a] e-mail: eboli@if.usp.br
[b] e-mail: tathagataghosh@hri.res.in (corresponding author)
[c] e-mail: matheus.martines.silva@usp.br
[d] e-mail: sujayshil1@gmail.com

Published online: 03 October 2025

we can realize the $SU(2)_L \otimes U(1)_Y$ symmetry linearly, *i.e.* we work in the Standard Model Effective Field Theory (SMEFT) framework. We choose the Hagiwara, Ishihara, Szalapski, and Zeppenfeld (HISZ) dimension-six basis [11–13] and we consider three operators contributing to TGC at dimension-six:

$$\begin{aligned} \mathcal{O}_W &= (D_\mu \Phi)^\dagger \widehat{W}^{\mu\nu} (D_\nu \Phi), \\ \mathcal{O}_B &= (D_\mu \Phi)^\dagger \widehat{B}^{\mu\nu} (D_\nu \Phi), \\ \mathcal{O}_{WWW} &= \mathrm{Tr}[\widehat{W}^\nu_\mu \widehat{W}^\rho_\nu \widehat{W}^\mu_\rho], \end{aligned} \tag{1}$$

where Φ stands for the SM Higgs doublet and we have defined $\widehat{B}_{\mu\nu} \equiv i(g'/2)B_{\mu\nu}$ and $\widehat{W}_{\mu\nu} \equiv i(g/2)\sigma^a W^a_{\mu\nu}$, with g and g' being the $SU(2)_L$ and $U(1)_Y$ gauge couplings, respectively. Here σ^a represents the Pauli matrices. In this work we considered the dimension-six effective lagrangian,

$$\mathcal{L}_{\text{eff}} = \mathcal{L}_{\text{SM}} + \frac{f_W}{\Lambda^2}\mathcal{O}_W + \frac{f_B}{\Lambda^2}\mathcal{O}_B + \frac{f_{WWW}}{\Lambda^2}\mathcal{O}_{WWW}, \tag{2}$$

where Λ is the characteristic mass scale of new physics and $f_{W,B,WWW}$ are Wilson coefficients. The above TGC operators can be qualitatively understood in terms of the effective γW^+W^- and ZW^+W^- parametrization introduced in Ref. [14]

$$\begin{aligned} \mathcal{L}_{WWV} = -ig_{WWV}\Big\{ & g_1^V \left(W^+_{\mu\nu} W^{-\mu} V^\nu - W^+_\mu V_\nu W^{-\mu\nu} \right) \\ & + \kappa_V W^+_\mu W^-_\nu V^{\mu\nu} + \frac{\lambda_V}{\widehat{M}_W^2} W^+_{\mu\nu} W^{-\nu\rho} V_\rho{}^\mu \Big\}, \end{aligned} \tag{3}$$

where $V = \gamma, Z$, $g_{WW\gamma} = \hat{e}$, $g_{WWZ} = \hat{e}\hat{c}/\hat{s}$, and $\widehat{M}_W = \hat{e}\hat{v}/2\hat{s}$, with $\hat{e}$ representing the proton electric charge and $\hat{c}(\hat{s})$ denoting the sine (cosine) of the weak mixing angle. In the SM, $g_1^\gamma = g_1^Z = \kappa_\gamma = \kappa_Z = 1$ and $\lambda_Z = \lambda_\gamma = 0$. After including the direct contribution from the dimension-six operators, electromagnetic gauge invariance still enforces $g_1^\gamma = 1$, while the other effective TGC couplings read:

$$\begin{aligned} \Delta g_1^Z &= \frac{\hat{e}^2}{8\hat{s}^2\hat{c}^2}\frac{\hat{v}^2}{\Lambda^2} f_W, \\ \Delta\kappa_\gamma &= \frac{\hat{e}^2}{8\hat{s}^2}\frac{\hat{v}^2}{\Lambda^2}\left(f_W + f_B\right), \\ \Delta\kappa_Z &= \frac{\hat{e}^2}{8\hat{s}^2}\frac{\hat{v}^2}{\Lambda^2}\left[f_W - \frac{\hat{s}^2}{\hat{c}^2} f_B\right], \\ \lambda_\gamma &= \lambda_Z = \frac{3\hat{e}^2}{2\hat{s}^2}\frac{\widehat{M}_W^2}{\Lambda^2} f_{WWW}. \end{aligned} \tag{4}$$

In addition to the TGC contributions, diboson production can also be modified by anomalous couplings of the gauge bosons to fermions. One important feature of the HISZ basis is that it does not give rise to blind directions in the electroweak precision observables (EWPO) at the Z pole in contrast to the Warsaw basis [15]. In fact, in the HISZ basis, EWPO lead to stringent bounds on the couplings of gauge bosons to fermions [16–20]. Hence, the present analysis of the diboson production is simplified because we can neglect anomalous fermion-gauge boson couplings due to the strong EWPO bounds on these couplings.

We simulate the EWDB channels at leading order using MadGraph5_aMC@NLO [21] with the UFO files for our effective Lagrangian generated with FeynRules [22,23]. We employ PYTHIA8 [24] to perform the parton shower and hadronization, while the fast detector simulation is carried out with Delphes [25]. Jet analyses are performed using FASTJET [26]. For the EWDB hadronic channels, the final jets were clustered and trimmed in the same way as described by the experimental collaborations [7,8], using the final state stable particles after performing the parton-shower and hadronization. The analysis of the jet-substructure was carried out using the plugins that are part of the FASTJET contrib project (https://fastjet.hepforge.org/contrib/). Moreover, we include next-to-leading order (NLO) QCD corrections by applying a bin-wise k-factor obtained using the SMEFT@NLO UFO package [27].

In this work, we considered two scenarios in our analyses. In the first scenario, we used the available Run 2 experimental data, which contains an integrated luminosity of 139 fb^{-1}. In the second scenario, we performed our analyses for the hadronic EWDB channels assuming the foreseen integrated luminosity of the High Luminosity LHC run, i.e. 3000 fb^{-1}, however, we kept the present experimental systematic errors.

Table 1 presents the Run 2 EWDB data used in our analyses, comprising a total of 92 data points, while, for the sake of comparison, we present in Table 2 the 95% CL limits observed by the LHC collaborations. Furthermore, in order to improve the statistical analysis of the hadronic channels, we rebinned the data. For the $W\gamma \to J\gamma$ channel, we merged the bins of the distribution in such a way that the total number of events in each bin can be described by a Gaussian distribution. For the ATLAS $WW/WZ \to 2J$ channel, the bins were combined to ensure at least one event per bin. In summary, the binnings used in our Run 2 analyses are as follows:

ATLAS $W\gamma \to J\gamma$ ($M_{J\gamma}$bins) :
(0.80, 0.88, 0.96, 1.04, 1.12, 1.20, 1.28, 1.36, 1.44, 1.52, 1.60, 1.68, 1.76, 1.84, 1.92, 2.00, 2.12, 2.28, 2.56, 2.96, 7.00) TeV

ATLAS $WW/WZ \to 2J$ (M_{JJ}bins) :
(1.30, 1.40, 1.50, 1.60, 1.70, 1.80, 1.90, 2.00, 2.10, 2.40, 3.10, 5.10) TeV.

On the other hand, our choice of bins for the HL-LHC analyses is

ATLAS $W\gamma \to J\gamma$ ($M_{J\gamma}$bins) :
(0.80, 0.92, 1.00, 1.08, 1.16, 1.24, 1.36, 1.48, 1.60, 1.72,

Table 1 EWDB data from LHC used in the analyses. For the W^+W^- results from ATLAS run 2 [28] we combine the data from the last three bins into one to ensure gaussianity

	Channel (a)	Distribution	# bins	Dataset	Int Lum
EWDB data	$WZ \to \ell^+\ell^-\ell'^{\pm}$	$M(WZ)$	7	CMS 13 TeV	137.2 fb^{-1} [2]
	$WW \to \ell^+\ell^{(\prime)-} + 0/1j$	$M(\ell^+\ell^{(\prime)-})$	11	CMS 13 TeV	35.9 fb^{-1} [3]
	$W\gamma \to \ell\nu\gamma$	$\frac{d^2\sigma}{dp_T d\phi}$	12	CMS 13 TeV	137.1 fb^{-1} [5]
	$WW \to e^{\pm}\mu^{\mp} + \not{E}_T$ $(0j)$	m_T	17 (15)	ATLAS 13 TeV	36.1 fb^{-1} [28]
	$WZ \to \ell^+\ell^-\ell^{(\prime)\pm}$	m_T^{WZ}	6	ATLAS 13 TeV	36.1 fb^{-1} [1]
	$WW \to \ell^+\ell^{(\prime)-} + \not{E}_T$ $(1j)$	$\frac{d\sigma}{dm_{\ell^+\ell^-}}$	10	ATLAS 13 TeV	139 fb^{-1} [4]
	$WW/WZ \to 2J$	M_{JJ}	11	ATLAS 13 TeV	139 fb^{-1} [7]
	$W\gamma \to J\gamma$	$M(J\gamma)$	20	ATLAS 13 TeV	139 fb^{-1} [8]

Table 2 Observed 95% CL allowed intervals for TGC Wilson coefficients from the datasets considered in our analyses. The constraints are given in TeV^{-2}

Channel	Dataset	f_B/Λ^2	f_W/Λ^2	f_{WWW}/Λ^2
$WZ \to \ell^+\ell^-\ell'^{\pm}$	CMS 13 TeV, 137.2 fb^{-1} [2]	[93 , 383.7]	[−3.11, 0.26]	[−4.20, 14.25]
$WW \to \ell^+\ell^{(\prime)-} + 0/1j$	CMS 13 TeV, 35.9 fb^{-1} [3]	[−9.4, 8.5]	[−3.6, 2.8]	[−1.8, 1.8]
$W\gamma \to \ell\nu\gamma$	CMS 13 TeV, 137.1 fb^{-1} [5]	–	–	[0.90 0.77]
$WW \to \ell^+\ell^{(\prime)-} + \not{E}_T$ $(1j)$	ATLAS 13 TeV, 139 fb^{-1} [4]	–	–	[−4.8, 4.8]

1.84, 1.96, 2.08, 2.20, 2.32, 2.44, 2.56, 2.68, 2.80, 2.96, 3.12, 3.28, 3.48, 3.76, 4.24, 7.00) TeV

ATLAS $WW/WZ \to 2J$ $(M_{JJ}\text{bins})$: (1.30, 1.40, 1.60, 1.80, 2.00, 2.20, 2.40, 2.60, 2.90, 3.40, 5.10) TeV.

In Fig. 1, we exhibit the anomalous TGC and background invariant mass distributions for the hadronic EWDB channels, choosing the values of the Wilson coefficients leading to 95% CL bounds in the given channel, along with the experimental data extracted from [7,8] for the Run 2 analysis. Notice that $\mathcal{O}_B$ and $\mathcal{O}_W$ contribute in the same way to $W\gamma$ production; see Eq. (4). As we can see, the presence of anomalous TGC enhances the cross section at large invariant masses. This behavior is expected, as the additional TGC contributions spoil the SM high-energy cancellations.

We performed the statistical analysis of the leptonic EWDB data using the binned chi-squared function described in Ref. [20]. On the other hand, for the analysis of the ATLAS $W\gamma \to J\gamma$ channel, we profited from the gaussianity of the combined bins and defined the chi-square function

$$\chi^2(f_B, f_W, f_{WWW}) = \min_{\vec{\xi}} \left\{ \sum_i \left(\frac{N_i^{\text{obs}} - N_i^{\text{th}}}{\sigma_i} \right)^2 + \xi_1^2 + \xi_2^2 \right\}, \tag{5}$$

where N_i^{obs} represents the observed number of events in the bin i while the theory prediction is given by

$$N_i^{\text{th}} = \left(1 + \sigma_{\xi_1}\xi_1\right) N_i^{\text{signal}} + \left(1 + \sigma_{\xi_2}\xi_2\right) N_i^{\text{backg}} \quad \text{with} \quad N_i^{\text{signal}} = N_i^{\text{int}} + N_i^{\text{BSM}}, \tag{6}$$

where N_i^{backg} denotes the number of background events extracted from Ref. [8], N_i^{int} stands for the expected number of events originating from the interference between the dimension-six operator and SM contributions, and N_i^{BSM} is the pure anomalous contribution to the number of expected events. Moreover, the σ_i contains the statistical and background uncertainties added in quadrature, given by $\sigma_i^2 = N_i^{\text{obs}} + \sigma_{\text{backg},i}^2$ where the last term in this expression was extracted from Ref. [8]. In order to account for possible systematic theoretical and experimental uncertainties, we defined two pulls [29], ξ_1 and ξ_2, affecting the normalization of the signal and background, respectively. The values chosen for σ_{ξ_1} and σ_{ξ_2} are 0.2 and 0.3, respectively. The values for σ_{ξ_1} and σ_{ξ_2} were estimated analysing the systematic errors from Ref. [8]. Although it is not possible to extract precise uncertainties from the available data, we made conservative estimates. Moreover, we expect the uncertainties on the signal to be slightly smaller than those on the background. In this case, an analytical expression for the pulls can be found by minimizing Eq. (5) with respect to ξ_1 and ξ_2.

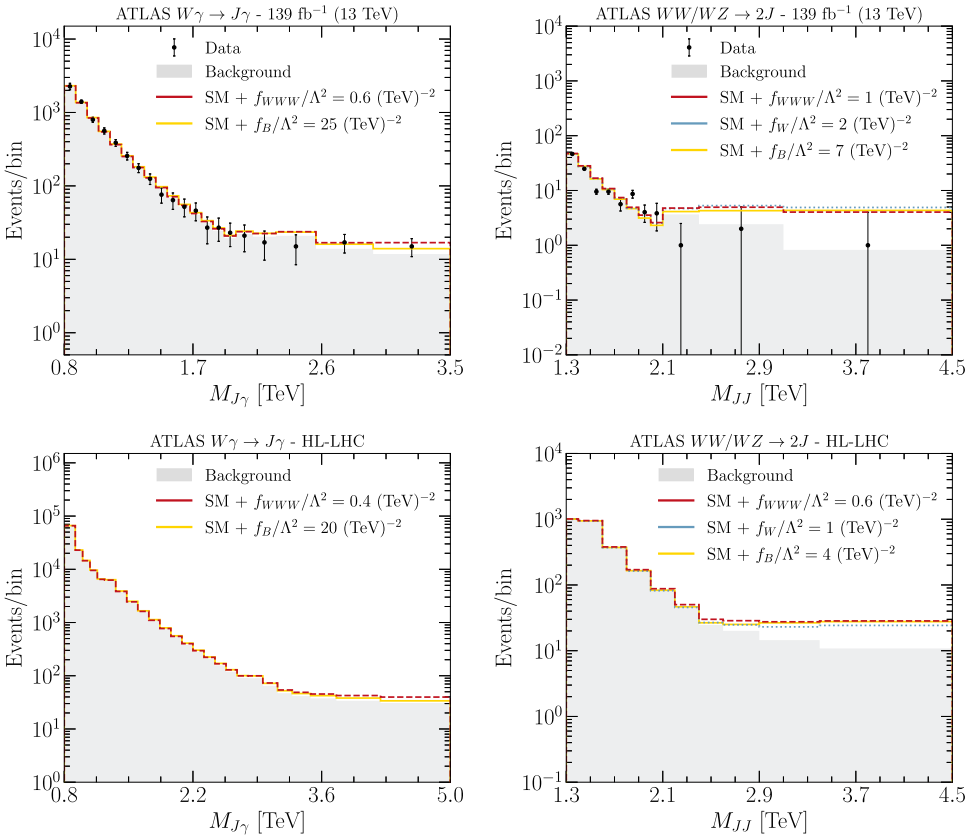

Fig. 1 Kinematical distributions employed in the hadronic analyses. The left (right) panels display the anomalous TGC and background $M_{J\gamma}$ (M_{JJ}) invariant mass distribution. On the first row, we present the distributions used for the Run 2 analyses, while on the bottom the ones used for the HL-LHC analyses. We used the fit to the background performed in the experimental analyses [7,8] for all of our studies, except that in the HL-LHC case, we rescaled it with the proper luminosity. On the left panels, the last bin contains events up to 7 TeV, while on the right panels, the last bin contains events up to 5.1 TeV

The statistical analyses of the ATLAS $WW/WZ \to 2J$ channel were based on the chi-square function [29]

$$\chi^2(f_B, f_W, f_{WWW}) = \min_{\vec{\xi}} \left\{ 2 \sum_i \left[N_i^{\rm th} - N_i^{\rm obs} + N_i^{\rm obs} \log\left(\frac{N_i^{\rm obs}}{N_i^{\rm th}}\right)\right] + \xi_1^2 + \xi_2^2 \right\}, \tag{7}$$

with $N_i^{\rm obs}$ standing for the observed number of events in the $i^{\rm th}$ bin and $N_i^{\rm th}$ defined as

$$N_i^{\rm th} = \left(1 + \sigma_i^{\xi_1} \xi_1\right) N_i^{\rm signal} + \left(1 + \sigma_i^{\xi_2} \xi_2\right) N_i^{\rm backg} \quad \text{with} \quad N_i^{\rm signal} = N_i^{\rm int} + N_i^{\rm BSM}, \tag{8}$$

where $N_i^{\rm backg}$, $N_i^{\rm int}$ and $N_i^{\rm BSM}$ represent the background-fit extracted from Ref. [7], and the linear and quadratic contributions of the dimension-six operators, respectively. Notice that we assume that the contributions of dimension-eight operators can be neglected, ergo introducing a model dependence in our analyses. For instance, for universal extensions of the standard model it has been shown that the impact of adding dimension-eight contributions to the analysis has a small impact [20].

The systematic uncertainties were parameterized by the nuisance parameters ξ_1 and ξ_2, which modify the normalization of the signal and background, respectively. We chose the values for $\sigma_i^{\xi_2}$ to best represent the experimental errors, and for $\sigma_i^{\xi_1}$, the values chosen stem from the theoretical uncertainties. Their values are

$$\sigma_i^{\xi_1} = (0.05, 0.05, 0.05, 0.05, 0.1, 0.1, 0.1, 0.15, 0.15, 0.15, 0.15), \tag{9}$$

$$\sigma_i^{\xi_2} = (0.1, 0.1, 0.2, 0.2, 0.4, 0.4, 0.5, 0.5, 1.0, 1.0, 1.0). \tag{10}$$

The HL-LHC analysis is carried out to estimate how the limits on the Wilson coefficients f_B, f_W and f_{WWW}, extracted using the hadronic EWDB channels, can improve with the upcoming LHC runs. Since there is no available data, we use the SM background fit scaled by a factor of 3000/139 as the observed number of events. As shown in the bottom row of Fig. 1, the number of events for each bin of the distributions for the $W\gamma$ and WW/WZ channels is sufficiently large, allowing us to assume gaussianity. To extract the 95% CL intervals, we use the same statistics defined in Eq. (5), with minor modifications to the uncertainties. For the ATLAS $W\gamma \to J\gamma$, we rescaled the $\sigma_{{\rm backg},i}$ to maintain the current $\sigma_{{\rm backg},i}/N_i^{\rm obs}$ ratio. For the ATLAS $WW/WZ \to 2J$, we defined $\sigma_{{\rm backg},i} = x_i N_i^{\rm backg}$, with

$$x_i = (0.1, 0.1, 0.2, 0.2, 0.4, 0.4, 0.5, 0.5, 1.0, 1.0), \tag{11}$$

to represent the same large uncertainties in the background as the current data.

Table 3 95% CL allowed intervals for the TGC Wilson coefficients originating from the different datasets. We marginalized the chi-square with respect to the other parameters in the analysis with the only exception being the $W\gamma$ channels for which we only included f_B since its contribution is identical to the f_W one, leading to a blind direction. In the fourth column we combined all the available data on WW and WZ production with the gauge bosons decaying to leptons. The allowed intervals are given in TeV^{-2}

Coefficient	Hadronic EWDB ($\mathcal{L} = 139\,\text{fb}^{-1}$)		Leptonic EWDB ($\mathcal{L} = 139\,\text{fb}^{-1}$)	
	ATLAS $WW/WZ \to 2J$	ATLAS $W\gamma \to J\gamma$	Combined WW/WZ	CMS $W\gamma \to \ell\nu\gamma$
$\frac{f_B}{\Lambda^2}$	$[-6.6, 6.9]$	$[-25, 25]$	$[-13, 15]$	$[-17, 19]$
$\frac{f_W}{\Lambda^2}$	$[-1.5, 1.8]$	$[-25, 25]$	$[-1.3, 2.5]$	$[-17, 19]$
$\frac{f_{WWW}}{\Lambda^2}$	$[-1.0, 1.0]$	$[-0.64, 0.64]$	$[-1.6, 1.6]$	$[-0.84, 0.74]$

3 Results

To estimate the LHC potential for studying TGC using highly boosted W's and Z's decaying hadronically, we recast the available ATLAS data on searches for resonances decaying into WW/WZ and $W\gamma$ pairs followed by the hadronic decays of the gauge bosons [7,8]. For comparison, we also obtained the Run 2 limits from combining fully leptonic modes; for details see Ref. [20].

Table 3 presents the 95% CL allowed intervals for the three TGC Wilson coefficients contributing to diboson production. In the second and third columns, we exhibit the results for the analysis performed using the hadronic WW/WZ production data and the hadronic $W\gamma$ results, respectively. For the sake of comparison, the fourth and fifth columns contain the allowed intervals using the leptonic final states of the WW/WZ and $W\gamma$ diboson productions. Taking into account only the fully hadronic final states, the Wilson coefficients f_B and f_W are better constrained by the WW/WZ diboson production. Additionally, f_{WWW} is more tightly constrained than f_W and f_B, with the $W\gamma$ production channel leading to the strongest bound. Comparing these results with those obtained from the leptonic decay modes, we can see that the fully hadronic channels lead to tighter limits on f_B due to the $2J$ final state. Moreover, the coefficients f_{WWW} and f_W are slightly better constrained by the hadronic channels. At this point it is interesting to contrast our results with the available ones from the LHC collaborations given in Table 2. As expected our combination of the leptonic channels leads to stronger constraints than the ones experimentally observed.[1] Clearly, the boosted jet analyses lead to more stringent limits on TGC than the presently available ones.

To compare the impact of the different datasets on the study of anomalous TGC, Fig. 2 depicts the 2σ allowed regions for all parameters in the analyses as well as the one-dimensional projection of the $\Delta\chi^2$. As we can see, the hadronic datasets lead to more stringent constraints on all coefficients in the analysis with f_B showing the most significant improvement; see Table 4 for the marginalized 95% CL allowed intervals. For all the hadronic (leptonic) results quoted in Table 4, we combine all the hadronic (leptonic) channels mentioned in Table 3. Notably, combining the WW/WZ and $W\gamma$ hadronic datasets breaks the blind direction $f_W + f_B$ that exists in the $W\gamma$ production. As could have been anticipated, the combination of the hadronic channels gives bounds on f_{WWW} similar to the ones originating from the leptonic final states; see Table 4. The combination of leptonic and hadronic channels leads, obviously, to more stringent limits.

We also obtained the attainable limits on the hadronic channel for the HL-LHC. We assumed that the observed number of events is the one predict by the fit to the SM background made by the ATLAS collaboration [7,8]. We also kept the same systematic uncertainties of this fit for the LHC Run 2 and we considered an integrated luminosity of 3000 fb^{-1}. Our results are presented in Table 5. As we can see, the HL-LHC can improve the present limits on the f_B, f_W, and f_{WWW} coefficients (see last column of Table 4) by almost a factor of 1.5 when we consider only the hadronic channels in contrast with the current leptonic limits.

4 Final remarks

We analyzed the LHC potential to probe anomalous TGC using the WW/WZ and $W\gamma$ channels when the W's and Z's decay hadronically. We considered boosted final states where the W/Z decay products give rise to a fat jet. In our analyses, we performed the same sequence of cuts used by the ATLAS collaboration for the search of heavy resonances [7, 8]. We also considered the SM background as evaluated in the experimental studies.

To gauge our results, we compared the limits of the TGC Wilson coefficients derived from the fully hadronic mode with the ones from the leptonic final state. Our results indi-

[1] We validated our analyses by reproducing the results obtained by collaborations for each dataset.

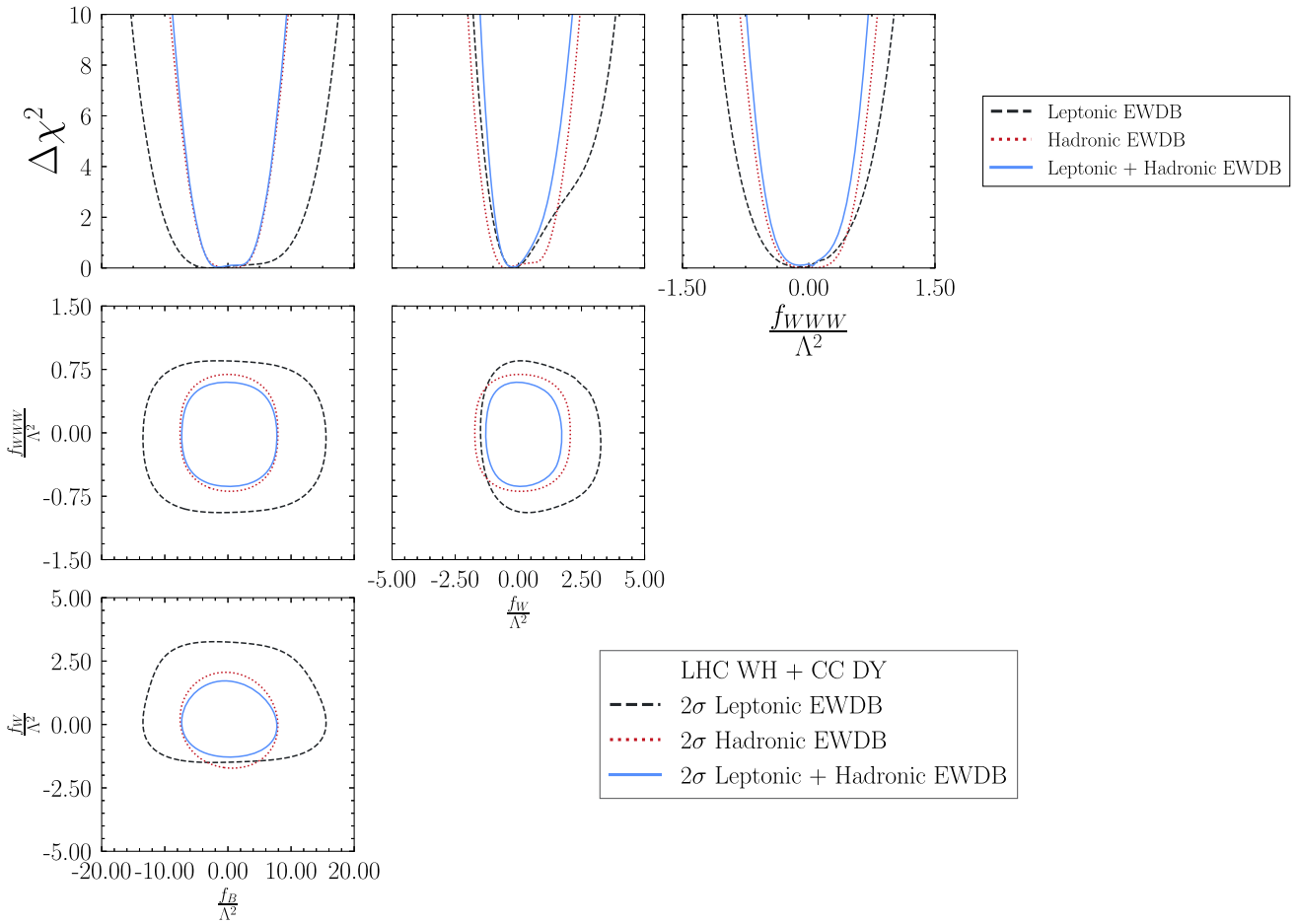

Fig. 2 1σ and 2σ allowed regions for each possible pair of Wilson coefficients in the analysis, after marginalizing over the undisplayed parameter, for the different datasets as indicated in the figure. We also display the one-dimensional marginalized projections of the $\Delta\chi^2$. The Wilson coefficients are given in TeV^{-2}

Table 4 95% CL allowed intervals for the TGC Wilson coefficients in the analysis of the hadronic channels, the result taking into account all leptonic channels, as well as the combination of leptonic and hadronic channels. In the hadronic (leptonic) results of this table we combine all the hadronic (leptonic) channels mentioned in Table 3 and the allowed intervals are given in TeV^{-2}

Coefficients	Hadronic EWDB ($\mathcal{L} = 139\,\text{fb}^{-1}$)	Leptonic EWDB ($\mathcal{L} = 139\,\text{fb}^{-1}$)	Leptonic + Hadronic EWDB ($\mathcal{L} = 139\,\text{fb}^{-1}$)
$\frac{f_B}{\Lambda^2}$	$[-6.5, 6.8]$	$[-12, 12]$	$[-6.3, 6.7]$
$\frac{f_W}{\Lambda^2}$	$[-1.5, 1.8]$	$[-1.3, 2.6]$	$[-1.1, 1.4]$
$\frac{f_{WWW}}{\Lambda^2}$	$[-0.61, 0.61]$	$[-0.83, 0.72]$	$[-0.57, 0.52]$

cate that the limits from leptonic and hadronic channels are similar. For instance, comparing the observed limits given in Table 2 with our results in Table 3 we learn that the hadronic limit improves the individually observed limits on f_B and f_W by a factor $\simeq 1.5$–2 while the hadronic limits on f_{WWW} can be tightened by a factor $\simeq 1.3$. Furthermore, the addition of the hadronic mode to the TGC analysis will lead to more stringent global fits; see Table 4. Given the present available luminosity, the bounds are driven by the TGC quadratic contributions, e.g. using only the linear terms on the anomalous couplings the hadronic results in Table 4 are soften to $f_B/\Lambda^2 \in [-116, 198]\,\text{TeV}^{-2}$, $f_W/\Lambda^2 \in [-0.1, 7.6]\,\text{TeV}^{-2}$ and $f_{WWW}/\Lambda^2 \in [-400., 0.0]\,\text{TeV}^{-2}$.

Anomalous TGC can be generated by integrating out new heavy states; however, the resulting anomalous couplings are suppressed by loop factors $1/(16\pi^2)$ for weakly interacting

Table 5 95% CL allowed intervals for the TGC Wilson coefficients for the hadronic model WW/WZ and $W\gamma$ as well as their combination. We assumed an integrated luminosity of 3000 fb^{-1} and the allowed intervals are given in TeV^{-2}

Coefficient	Hadronic EWDB ($\mathcal{L} = 3000\,\text{fb}^{-1}$)		
	ATLAS WW/WZ	ATLAS $W\gamma$	Combined WW/WZ and $W\gamma$
$\frac{f_B}{\Lambda^2}$	$[-3.7, 4.0]$	$[-15, 16]$	$[-3.7, 4.0]$
$\frac{f_W}{\Lambda^2}$	$[-0.8, 1.1]$	$[-15, 16]$	$[-0.8, 1.1]$
$\frac{f_{WWW}}{\Lambda^2}$	$[-0.6, 0.6]$	$[-0.3, 0.3]$	$[-0.3, 0.3]$

extensions of the SM [30]. Considering a weakly coupled BSM scenario, the present and future TGC limit of the order of 1 TeV translates into a new physics mass scale of the order of 100 GeV or less. The LHC is certainly not probing this kind of scenario; otherwise, we would have already observed these new particles directly. On the other hand, for a strongly coupled UV completion with a coupling $g_\star = \sqrt{4\pi}$ the limits on TGC exclude new physics lighter than 10 TeV.

Finally, we should conclude by reiterating the fact that the results presented in this paper relies heavily on the experimental fit to the SM background and the fits have large systematic uncertainties. In fact, this even leaves a room for improvement if the systematic uncertainties can be reduced for the high luminosity run of the LHC.

Acknowledgements We would like to thank Najimuddin Khan for useful discussions in the early part of the project. OJPE is partially supported by CNPq grant number 305762/2019-2 and FAPESP grant 2019/04837-9. TG would like to acknowledge support from the Department of Atomic Energy, Government of India, for Harish-Chandra Research Institute. MM is supported by FAPESP grant number 2022/11293-8. SS is supported by FAPESP Grant number 2021/09547-9.

Data Availability Statement Data will be made available on reasonable request. [Authors' comment: The datasets generated during and/or analysed during the current study are available from the corresponding author on reasonable request. The authors reserve the right to determine whether a request is reasonable.]

Code Availability Statement Code/software will be made available on reasonable request. [Authors' comment: The code/software generated during and/or analysed during the current study is available from the corresponding author on reasonable request. The authors reserve the right to determine whether a request is reasonable.]

Funded by SCOAP^3.

References

1. ATLAS Collaboration, Measurement of $W^\pm Z$ production cross sections and gauge boson polarisation in pp collisions at $\sqrt{s} = 13$ TeV with the ATLAS detector. ATLAS-CONF-2018-034 (2018). https://cds.cern.ch/record/2630187
2. CMS Collaboration, Measurement of the pp $\rightarrow$ WZ inclusive and differential cross sections, polarization angles and search for anomalous gauge couplings at $\sqrt{s} = 13$ TeV. CMS-PAS-SMP-20-014 (2021). https://cds.cern.ch/record/2758362
3. A.M. Sirunyan et al., Phys. Rev. D **102**(9), 092001 (2020). https://doi.org/10.1103/PhysRevD.102.092001
4. G. Aad et al., JHEP **06**, 003 (2021). https://doi.org/10.1007/JHEP06(2021)003
5. CMS Collaboration, CMS-PAS-SMP-20-005 (2021). https://cds.cern.ch/record/2757267
6. M. Aaboud et al., Eur. Phys. J. C **77**(8), 563 (2017). https://doi.org/10.1140/epjc/s10052-017-5084-2
7. G. Aad et al., JHEP **09**, 091 (2019). https://doi.org/10.1007/JHEP09(2019)091. [Erratum: JHEP **06**, 042 (2020)]
8. G. Aad et al., JHEP **07**, 125 (2023). https://doi.org/10.1007/JHEP07(2023)125
9. G. Aad et al., Phys. Lett. B **716**, 1 (2012). https://doi.org/10.1016/j.physletb.2012.08.020
10. S. Chatrchyan et al., Phys. Lett. B **716**, 30 (2012). https://doi.org/10.1016/j.physletb.2012.08.021
11. K. Hagiwara, S. Ishihara, R. Szalapski, D. Zeppenfeld, Phys. Rev. D **48**, 2182 (1993). https://doi.org/10.1103/PhysRevD.48.2182
12. K. Hagiwara, T. Hatsukano, S. Ishihara, R. Szalapski, Nucl. Phys. B **496**, 66 (1997). https://doi.org/10.1016/S0550-3213(97)00208-3
13. T. Corbett, O.J.P. Éboli, J. González-Fraile, M.C. González-Garcia, Phys. Rev. D **87**, 015022 (2013). https://doi.org/10.1103/PhysRevD.87.015022
14. K. Hagiwara, R.D. Peccei, D. Zeppenfeld, K. Hikasa, Nucl. Phys. B **282**, 253 (1987). https://doi.org/10.1016/0550-3213(87)90685-7
15. B. Grzadkowski, M. Iskrzynski, M. Misiak, J. Rosiek, JHEP **10**, 085 (2010). https://doi.org/10.1007/JHEP10(2010)085
16. A. Butter, O.J.P. Éboli, J. Gonzalez-Fraile, M.C. Gonzalez-Garcia, T. Plehn, M. Rauch, JHEP **07**, 152 (2016). https://doi.org/10.1007/JHEP07(2016)152
17. E. da Silva Almeida, A. Alves, N. Rosa Agostinho, O.J.P. Éboli, M.C. Gonzalez-Garcia, Phys. Rev. D **99**(3), 033001 (2019). https://doi.org/10.1103/PhysRevD.99.033001

18. A. Alves, N. Rosa-Agostinho, O.J.P. Éboli, M.C. Gonzalez-Garcia, Phys. Rev. D **98**(1), 013006 (2018). https://doi.org/10.1103/PhysRevD.98.013006
19. E.d.S. Almeida, A. Alves, O.J.P. Éboli, M.C. Gonzalez-Garcia, (2021)
20. T. Corbett, J. Desai, O.J.P. Éboli, M.C. Gonzalez-Garcia, M. Martines, P. Reimitz, Phys. Rev. D **107**(11), 115013 (2023). https://doi.org/10.1103/PhysRevD.107.115013
21. R. Frederix, S. Frixione, V. Hirschi, D. Pagani, H.S. Shao, M. Zaro, JHEP **07**, 185 (2018). https://doi.org/10.1007/JHEP07(2018)185
22. N.D. Christensen, C. Duhr, Comput. Phys. Commun. **180**, 1614 (2009). https://doi.org/10.1016/j.cpc.2009.02.018
23. A. Alloul, N.D. Christensen, C. Degrande, C. Duhr, B. Fuks, Comput. Phys. Commun. **185**, 2250 (2014). https://doi.org/10.1016/j.cpc.2014.04.012
24. T. Sjostrand, S. Mrenna, P.Z. Skands, Comput. Phys. Commun. **178**, 852 (2008). https://doi.org/10.1016/j.cpc.2008.01.036
25. J. de Favereau, C. Delaere, P. Demin, A. Giammanco, V. Lemaitre, A. Mertens, M. Selvaggi, JHEP **02**, 057 (2014). https://doi.org/10.1007/JHEP02(2014)057
26. M. Cacciari, G.P. Salam, G. Soyez, Eur. Phys. J. C **72**, 1896 (2012). https://doi.org/10.1140/epjc/s10052-012-1896-2
27. C. Degrande, G. Durieux, F. Maltoni, K. Mimasu, E. Vryonidou, C. Zhang, Phys. Rev. D **103**(9), 096024 (2021). https://doi.org/10.1103/PhysRevD.103.096024
28. M. Aaboud et al., Eur. Phys. J. C **78**(1), 24 (2018). https://doi.org/10.1140/epjc/s10052-017-5491-4
29. G.L. Fogli, E. Lisi, A. Marrone, D. Montanino, A. Palazzo, Phys. Rev. D **66**, 053010 (2002). https://doi.org/10.1103/PhysRevD.66.053010
30. C. Arzt, M.B. Einhorn, J. Wudka, Nucl. Phys. B **433**, 41 (1995). https://doi.org/10.1016/0550-3213(94)00336-D